2015 International Conference on Computational Science and Computational Intelligence

Applied Machine Learning to Identify Alzheimer's Disease Through the Analysis of Magnetic Resonance Imaging

Elva María Novoa-del-Toro
Universidad Veracruzana
Xalapa, Veracruz, Mexico
elvamaria@gmail.com

Juan Fernández-Ruiz
Universidad Autónoma de México
Ciudad de Mexico, D.F., Mexico

Héctor Gabriel Acosta-Mesa
Universidad Veracruzana
Xalapa, Veracruz, Mexico

Nicandro Cruz-Ramírez
Universidad Veracruzana
Xalapa, Veracruz, Mexico

***Abstract*—Alzheimer's disease is among the most common neurodegenerative diseases [1], doubling the number of patients every 5-year interval beyond age 65 [2]. Different investigations have proven that patients with Alzheimer's disease, show volume reduction at specific areas of the brain [1, 3-11]. Some of these areas, like the precuneus, start showing atrophy since early stages of the disease [1, 3, 6, 12-14], as measured through the use of Magnetic Resonance Imaging [9]. Considering this, we studied the possible use of the precuneus as a biomarker to identify such disease. Our results suggest that the precuneus is a potential biomarker to detect Alzheimer's disease, since 7 out of 10 patients (73.33% of accuracy) can be correctly classified.**

Keywords- Alzheimer's disease; precuneus; biomarker; classification; Magnetic Resonance Imaging.

I. INTRODUCTION

Alzheimer's disease (AD) is among the most common neurodegenerative illnesses [1], doubling the number of patients every 5-year interval beyond age 65 [2]. AD causes cognitive deterioration and behavioral disorders, while its most characteristic symptom is memory loss. AD is also the most common cause of dementia during old age [1-5, 15-17]. In general, AD develops in people older than 60 years old [2].

Different investigations have shown that patients with AD have volume reduction in specific areas of the brain [1, 3-11], although AD is not the only disease that causes loss of cerebral volume.

It is possible to observe this atrophy directly and non-invasively through Magnetic Resonance Imaging (MRI) [9]. This variable has been used as a biomarker to detect AD at different stages of the disease, with accuracies between 74 and 94% [1, 3, 6, 12-16, 18-24]. Although many different techniques have been investigated to try to predict the presence of AD, they all focus on the study of the hippocampus; notwithstanding other areas also show such atrophy, including the precuneus [1, 3, 6, 12-14].

Considering that the reduction of the precuneus volume is associated with early stages of AD, and the importance that this region could have to improve the predictive index of such illness, in this work we studied the use of the precuneus as a biomarker to identify AD, analyzing its features visualized through MRI.

II. PREVIOUS WORK

During the last decade many approaches that analyze anatomical MRI have been developed to classify patients with AD or Mild Cognitive Impairment (MCI) [1, 3, 6, 12-16, 18-24]. In general, these methods analyze the whole brain, a single section or a group of them. It is important to mention that, until some years ago, the only way to confirm if a person had AD was at autopsy [5, 17]. Fortunately, nowadays there is a diversity of non-invasive techniques that can be used to diagnose AD while the patient is still alive. The goal is to detect this illness as soon as possible (during early stages), so that the quality of life of the patient can be improved.

Hinrichs et al. [16] proposed to boost the MRI classification by segmenting the brain in: white matter, gray matter and cerebrospinal fluid. Their goal was to increase the accuracy of weak classifiers (those with low classification accuracy), using a group of them to discriminate between healthy controls and AD patients. Their premise was that, if the errors of those weak classifiers had no correlation between them, the combination of many classifiers would increase the general accuracy. Considering each MRI's voxel as a weak classifier, they tried to find a correlation between the voxels intensity changes in the same position in the MRI of all the subjects and the AD diagnosis. Then they assigned a weight to each voxel according to the classification result and finally they selected those voxels with the highest accuracy, using an algorithm designed to prefer contiguous groups and to avoid isolated voxels. Using a sample of 183 subjects from the ADNI database, they got a maximum accuracy of 84%.

A different approach developed by Plant et al. [3] analyzed MRIs images using a Support Vector Machine (SVM), a Bayesian classifier and voting feature intervals. They obtained the minimum set of voxels needed to predict the AD diagnosis vs. MCI or healthy control participants. They analyzed the whole brain of 32 patients with AD, 24 with MCI and 18

978-1-4673-9795-7/15 $31.00 © 2015 IEEE
DOI 10.1109/CSCI.2015.143

controls. Their classification accuracy of AD vs healthy controls was 92%.

A number of studies have used shapes to classify AD patients. Costafreda et al. [18] analyzed the shape of the hippocampus to predict the conversion from MCI to AD, using 103 subjects with MCI. They automatically segmented a Region of Interest (ROI), i.e. the hippocampus, through an auto context model, which is a pattern recognition algorithm, developed by Morra, et al. [25], specifically to make an automatic segmentation of the hippocampus. Then, they built a net shaped 3-D representation of the segmented ROI and mapped it into a common triangulation net, finding the correspondence of every vertex between subjects and thus, making a local statistical analysis among subjects. They used SVM to classify and obtained 80% of accuracy.

Similarly, Gutman et al. [20] also analyzed the shape of the hippocampus to detect AD. They built triangular net models of the global hippocampus shape of 49 AD patients and 63 healthy controls and created an invariant description of each shape. Then they used a SVM to classify and achieved 82.1% of accuracy.

Gerardin et al. [6] grouped 23 MCI and 23 AD patients and distinguished them from 25 healthy controls, using features of the shape of the hippocampus, obtained through spherical harmonics coefficients. They used SVM to do the classification with 94% of accuracy.

On the other hand, Ferrarini et al. [9] used independently the shape and volume of the hippocampus to diagnose AD. They modeled the hippocampus of 50 AD patients, 30 MCI subjects and 50 healthy controls, using a software they developed, which represents the volume of interest as a net, where each node is associated with a specific node of the rest of the hippocampus models. They obtained 74% of accuracy, using the volume and the precuneus and 90% with the shape of the ROI.

The pattern approach that Fan et al. [5] proposed was high dimensional. They considered all brain regions to identify those whose joint volumes maximized the difference between patients with MCI or AD and healthy controls. They selected two regions: the hippocampus and the entorrinal cortex and used a sample of 66 controls, 88 MCI and 56 AD, from the ADNI database. They did tests with the three groups, as follows: AD vs controls (82%), MCI vs controls (76%) and AD vs MCI (58.3%). They concluded that their accuracies (listed between brackets in every case), were not good enough to make a clinical diagnostic.

Vemuri et al. [19] used a SVM and the whole brain volume of 140 AD patients and 140 healthy controls, to calculate a structural abnormality index. They distinguished between controls and AD patients with an accuracy of 89.3%.

Since the precuneus is a brain region that has not been yet explored to diagnose AD, even though its atrophy is associated even with early stages of AD, in this work, we used the precuneus to determine if its features help to differentiate between healthy controls and AD patients.

III. MATERIALS AND METHODS

We analyzed 30 high resolution MRI's: 15 of healthy controls and 15 of AD patients.

Our methodology consisted of five main steps:

A. *MRI acquisition*

All the subjects were between 40 and 90 years old. All the participants complied with MRI safety standards. For the AD participants only mild AD patients were included (Montreal Cognitive Assessment –MoCA-, score greater or equal to 18/30).

B. *Manual segmentation of the precuneus in the MRI's native space*

We used ITK-SNAP, an open source tool [26] to do a manual segmentation of the precuneus. The segmentation followed the anatomical guidelines described in [2] and were marked in the sagittal plane first and then segmented in the coronal plane of the native space MRI's. Figures 1 and 2 show the manually segmented volumes of a healthy control and an AD patient, respectively.

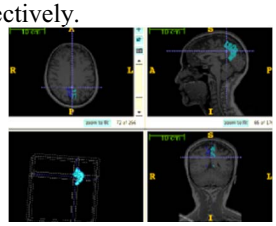

Fig. 1. 3D reconstruction of a manual segmentation of the precuneus of a healthy participant using ITK SNAP.

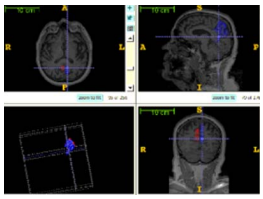

Fig. 2. 3D reconstruction of a manual segmentation of the precuneus of an AD patient using ITK SNAP.

C. *Standardization of the MRI volumes to Talairach coordinates*

We used BrainVoyager, a neurology specialized software [27], to standardize all images to Talairach coordinates. This stage had two steps: first, we localized the coordinates of the Anterior (AC) and Posterior Commissures (PC), to position the brain into the AC-PC plane. This locates the brain into a common origin and eliminates the implicit rotation, acquired during the MRI scan, where the heads of the participants can vary between scans.

After that, we localized the coordinates of the six points that delimitate the brain: AP (most anterior point), PP (most posterior point), SP (superior point), IP (inferior point), RP (most right point) and LP (most left point).

After the standardization, the brains had similar rotations, translations and dimensions (length, width and height), as shown in Figure 3, where a segmented volume of the precuneus is presented, before and after the standardization.

a) Before standardization. b) After standardization.

Fig 3. 3D reconstruction of the precuneus (showed in blue) of an AD patient, in its real location inside the brain (showed as a transparent net).

D. Feature selection

We represented the segmented volumes with a vector of 44 features (Table I), which describe the shape of the precuneus at different level of detail.

TABLE I. DESCRIPTION OF THE VECTOR OF FEATURES

Type	Description	Size
Basic measures	Define the shape of the precuneus in a basic level. This group is conformed by: volume and perimeter.	2
Central moments of the sagittal, axial and coronal planes	Allow to make a position independent description of the precuneus. This group is conformed by $\eta_{2,0}, \eta_{1,1}, \eta_{0,2}, \eta_{1,2}, \eta_{2,1}, \eta_{3,0}$ and $\eta_{0,3}$ (refer to equation 4).	21
Invariant moments of the sagittal, axial and coronal planes	Allow to make a size and angle independent description of the precuneus. This group is conformed by $h_1, h_2, h_3, h_4, h_5, h_6$ and h_7 (refer to equations 5-11).	21

In this case, the volume is the total percentage of the brain that the precuneus represents. To calculate the volume, we counted the number of voxels that belong to the brain and precuneus, independently and obtained the proportion between them. On the other hand, to calculate the perimeter, we counted the voxels that are part of the precuneus and that at least one of its 26 neighbors [28], belongs to the background, i.e. it is not part of the precuneus.

The central and invariant moments [29, 30], are used in the field of computer vision, to describe objects. Moments are measures related to the size, orientation and shape of an object.

The moment of $p + q$ order of an image $I(x, y)$ is [29]:

$$M_{p,q} = \sum_{x=1}^{Col} \sum_{y=1}^{Row} x^p y^q I(x, y) \quad (1)$$

where,

Col and Row are the image dimensions: columns and rows, respectively,

p and q are positive integers or equal to cero, which determine the order of the moment, and

x and y are the coordinates of the image I.

The center of gravity $(\bar{x}, \bar{y})$ of an image I, is calculated using the moments of order zero and one [29], as follows:

$$\bar{x} = \frac{M_{1,0}}{M_{0,0}} \qquad \bar{y} = \frac{M_{0,1}}{M_{0,0}} \quad (2)$$

The μ central moments, of $p + q$ order, allow describing an object, independently of its position and are calculated with respect to the center of gravity [29]:

$$\mu_{p,q} = \sum_{x=1}^{Col} \sum_{y=1}^{Row} (x - \bar{x})^p (y - \bar{y})^q I(x, y) \quad (3)$$

In order to get a description independent of the size of the object, we normalized the central moments, with respect to the zero moment, which is the area of the object [29]:

$$\eta_{p,q} = \frac{\mu_{p,q}}{M_{0,0}^{\alpha}} \qquad \alpha = \frac{p+q}{2} + 1 \quad (4)$$

Finally, with the normalized central moments, of orders two and three, we calculated the invariant moments $h_1, h_2, \ldots, h_7$, which are independent of the position, size and rotation of the object [29]:

$$h_1 = \eta_{2,0} + \eta_{0,2} \quad (5)$$

$$h_2 = (\eta_{2,0} - \eta_{0,2})^2 + 4{\eta_{1,1}}^2 \quad (6)$$

$$h_3 = (\eta_{3,0} - 3\eta_{1,2})^2 + (3\eta_{2,1} - \eta_{0,3})^2 \quad (7)$$

$$h_4 = (\eta_{3,0} + \eta_{1,2})^2 + (\eta_{0,3} + \eta_{2,1})^2 \quad (8)$$

$$h_5 = (\eta_{3,0} - 3\eta_{1,2})(\eta_{3,0} + \eta_{1,2})[(\eta_{3,0} + \eta_{1,2})^2 - 3(\eta_{0,3} + \eta_{2,1})^2] + (3\eta_{2,1} - \eta_{0,3})(\eta_{0,3} + \eta_{2,1})[3(\eta_{3,0} + \eta_{1,2})^2 - (\eta_{0,3} + \eta_{2,1})^2] \quad (9)$$

$$h_6 = (\eta_{2,0} - \eta_{0,2})[(\eta_{3,0} + \eta_{1,2})^2 - (\eta_{0,3} + \eta_{2,1})^2] + 4\eta_{1,1}(\eta_{3,0} + \eta_{1,2})(\eta_{0,3} + \eta_{2,1}) \quad (10)$$

$$h_7 = (3\eta_{2,1} - \eta_{0,3})(\eta_{3,0} + \eta_{1,2})[(\eta_{3,0} + \eta_{1,2})^2 - 3(\eta_{0,3} + \eta_{2,1})^2] - (\eta_{3,0} - 3\eta_{1,2})(\eta_{0,3} + \eta_{2,1})[3(\eta_{3,0} + \eta_{1,2})^2 - (\eta_{0,3} + \eta_{2,1})^2] \quad (11)$$

Given these definitions, we obtained the binary images of the sagittal, axial and coronal cuts (from now on: lateral, superior and frontal views, respectively), of every segmented volume, so that we could see the precuneus from three different angles. Refer to figures 4 to 6 for a 3D representation of these views, where the brain is represented as a transparent net and the precuneus is showed in blue color.

It is worth mentioning that, after the standardization to Talairach coordinates, there is no rotation left. Therefore, these binary views provide a more detailed description of the shape of the precuneus, compared with the one obtained with the basic metrics.

a) Lateral view of a healthy control. b) Lateral view of an AD patient.

Fig. 4. Lateral view in 3D (sagittal plane).

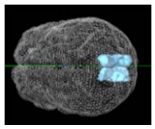
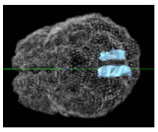

a) Superior view of a healthy control. b) Superior view of an AD patient.

Fig. 5. Superior view in 3D (axial plane).

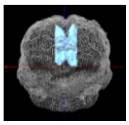
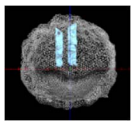

a) Frontal view of a healthy control. b) Frontal view of an AD patient.

Fig. 6. Frontal view in 3D (coronal plane).

Considering that the classification accuracy can decrease due to the different range of values of the features and their standard deviation, we normalized the feature vector, with the following equation [31]:

$$v_n = \frac{v_i - \min(v_1 \ldots v_n)}{\max(v_1 \ldots v_n) - \min(v_1 \ldots v_n)} \quad (12)$$

where,

v_n is the normalized value, within the range [0, 1],

v_i is the i-th value of the feature,

$\min(v_1 \ldots v_n)$ is the minimum value of the feature, and

$\max(v_1 \ldots v_n)$ is the maximum value of the feature.

E. Classification

For the classification phase, we used four methods: Support Vector Machines (SVM) [46], Naïve Bayes (NB), Decision Trees (DT) [47-49] and k-Nearest Neighbors (k-NN) -with k=1, 3 and 5-. All of which are available in WEKA (Waikato Environment for Knowledge Analysis), an open source software [32].

In general, SVM allows creating a model able to separate linear and non-linear data. NB uses probability to determine the class of a given instance, while DT builds a tree, which, depending on its complexity (depth and width) allows separating non-linear data. Finally, k-NN uses the similarity (short distance) of a new unclassified instance, with the classes of its neighbors, to determine which class the new instance is more likely to belong.

We chose those four classifiers because, according to the computer science literature, they have been used to solve different types of issues, with a good performance (high level of accuracy), depending on the problem.

Considering that each of the four classifiers uses different techniques and assumptions to obtain a result, it is interesting to compare their performance for a particular case, since there is not a universal machine-learning scheme that can be appropriate for all data mining problems [33].

On the other hand, to test the efficacy of each of the classifiers, we used cross-validation and we compared their results using two statistical tests: Kruskal Wallis and Wilcoxon.

IV. Results

We started our experiments with the extraction and normalization (to oscillate within the range [0, 1]) of the 44 features of every participant. Then, we generated the scatter plots of both, the original and the normalized values. We show some examples of the scatter plots in figures 7 to 11, where AD cases are marked with red colored "+" and the healthy controls are represented in blue colored "o".

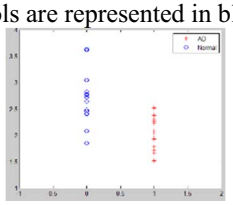
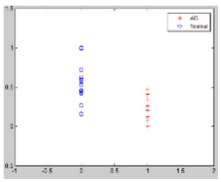

a) Original values. b) Normalized values.

Fig. 7. Scatter plots of the volume feature.

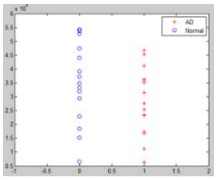
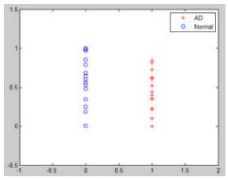

a) Original values. b) Normalized values.

Fig. 8. Scatter plots of the invariant moment h2, of the frontal view.

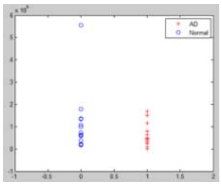
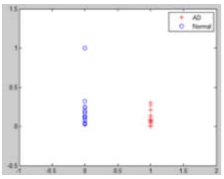

a) Original values. b) Normalized values.

Fig. 9. Scatter plots of the invariant moment h3, of the superior view.

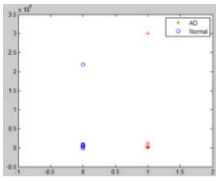
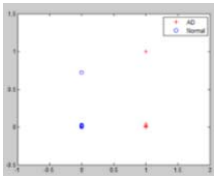

a) Original values. b) Normalized values.

Fig. 10. Scatter plots of the invariant moment h4, of the lateral view.

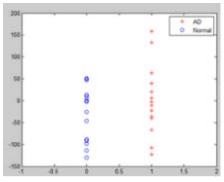
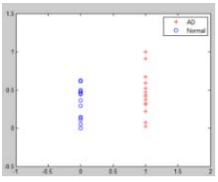

a) Original values. b) Normalized values.

Fig. 11. Scatter plots of the central moment $\eta_{3,0}$, of the superior view.

For the classification experiments, we used the normalized values of the 44 dimensional vectors of the 30 segmented volumes of the precuneus. To validate the results, we used

cross validations, with 5 stratified folds and 30 folds (leave-one-out).

We did 30 repetitions of the experiment and we obtained the best results using 5 folds, where the accuracy range oscillated between 46.67% (NB) and 86.67% (DT), in the worst and best cases, respectively. A statistic summary of the results for DT (best accuracy), is presented in Table II.

TABLE II. STATISTIC SUMMARY OF THE RESULTS OBTAINED WITH DECISION TREES

Statistic summary	Decision Trees (5 folds)		
	Sensibility	*Specificity*	*Accuracy*
Best	86.67%	86.67%	86.67%
Worst	40.00%	66.67%	60.00%
Mean	63.78%	82.89%	73.33%
Median	66.67%	86.67%	73.33%
Standard Deviation	10.4582	5.9842	5.8722

In order to verify if there were significant differences between the results obtained with each classifier, we performed the statistical tests Wilcoxon and Kruskal Wallis, with the accuracies of the 30 executions, obtained by the four classifiers. We chose to use the accuracy because it represents a compromise between sensibility and specificity, in a way that the accuracy can only be high, if the other two metrics are also high.

We found that in almost all the cases, there is a statistical significant difference between the results of every pair wise of classifiers, with 95% of confidence. In the case of five folds, the only exceptions are the comparatives between the following pairs: NB/k-NN, with k=1; k-NN, with k=3/k-NN, with k=5. On the other hand, with thirty folds, the only non-significant difference is between DT/k-NN, with k=3.

V. DISCUSSION

Here we explored the use of a potential biomarker to detect AD. We used a 44-dimensional vector representation of the precuneus' shape and size to try to distinguish between AD and Normal (healthy controls) classes.

We found five particularities in the scatter plots:

1) Features showing a certain degree of separability for the Normal class.

2) Features where the majority of the instances of both classes shared the same range.

3) Cases where one or more instances of any of the classes were notably separated from the rest.

4) Features where the instances were located in only three or four different areas.

5) Cases where the instances of the same class were scattered in a way that, they form groups, with an almost uniform intragroup distance and a notable intergroup distance.

Figure 7 shows an example of the first case in the volume attribute, where a group of instances of the Normal (healthy controls) class, were out of the range of the AD class. This suggests some degree of separability, although the majority of the instances of the AD class were within the same range as the Normal class.

In contrast, Figure 8 illustrates the second case, where most of the instances of both classes shared the same range.

The third case is exemplified in Figure 9, where one of the instances of the Normal class is isolated from the rest. This somehow suggests the presence of outliers, which could imply noise in the data.

The fourth case can be seen in Figure 10, where all the instances are located in three areas, two of which seem to be outliers. The fact that most of the instances of both classes are almost in the same spot, suggest that, at least for these particular features, the AD patients and the healthy controls share the same properties, and therefore they will not help to distinguish between the two classes. If these possible outliers that have this particularity came from the same MRI's, it could imply that these particular manual segmentations of the precuneus were inaccurate.

Finally, the fifth case group formation, shown in Figure 11, could suggest that we used a small sample. It could be possible that a sample increase would lead to find instances corresponding with the values that now separate the groups; considering the course of dimensionality, due to the size of the sample is small, compared with the number of features.

The fact that there is a statistically significant difference between the results of almost every pair of classifiers, implies that, with a 95% level of confidence, we can sustain that for our data sample and the classification experiments performed with the normalized values of the 44 features, the DT classifier is the best option, due to its maximum accuracy of 86.67%. This performance is comparable with the results of some of the other studies previously mentioned, e.g. the 84% accuracy reported by Hinrichs et al. [16], the 82.1% by Gutman et al. [20] and the 82% by Fan et al. [5]. However, the mean accuracy obtained with DT is 73.33%, which is below the one reported by these authors.

The highest mean accuracy (73.33%) and the maximum accuracy (86.67%) were obtained with DT. Therefore, between seven and eight out of every ten MRI volumes, are correctly classified. Nonetheless, there are other techniques which results are more competitive that our mean accuracy, like those reported by: Fan et al. [5] (82%), Gutman, et al. [20] (82.1%), Hinrichs et al. [16] (84%), Vemuri et al. [19] (89.3%), Ferrarini et al. [9] (90%), Plant et al. [3] (92%), Gerardin et al. [6] (94%).

On the other hand, none of those works reported the AD stage of their participants, while we only considered patients in an early AD stage. This suggests that it could be possible that the precuneus allows identifying this illness even before the hippocampus shows anatomical changes. That is, when AD is still incipient.

VI. CONCLUSIONS AND FUTURE WORK

Our results suggest that the 44 characteristics of the precuneus, visualized through MRI allow differentiating between healthy controls and AD patients, with a mean sensibility of 63.78% and a specificity of 82.89%, which gives 73.33% of accuracy. This implies that around seven out of ten patients are correctly classified.

However, as mentioned in the previous section, other techniques give better classification results. Nonetheless, the proposed method combined with other methods, could help as adjuvant in the detection of AD, improving the general accuracy.

As future work, in an attempt to improve the sensibility, we plan to describe the precuneus using tridimensional features. Additionally, we plan to reduce the dimensionality with methods like Naïve Bayes, to obtain the conditional probability of correctly calculate the class, given a certain feature, in a way that we can omit approaching probability zero.

REFERENCES

[1] Ryu S.Y., Kwon M.J., Lee S.B., Yang D.W. Kim T.W., Song I.U., et. al.: Measurement of Precuneal and Hippocampal Volumes Using Magnetic Resonance Volumetry in Alzheimer's Disease. Journal of Clinical Neurology 6 (4), 196-203 (2010)

[2] NINDS Fact sheet. Dementia: Hope Through Research. http://www.ninds.nih.gov/disorders/dementias/detail_dementia.htm

[3] Plant C., Teipel S.J., Oswald A., Böhm C., Meindl T., et. al.: Automated Detection of Brain Atrophy Patterns Based on MRI for the Prediction of Alzheimer's Disease. NeuroImage 50, Issue 1, 162-174 (2010)

[4] Zarei M., Patenaude B., Damoiseaux J., Morgese C., Smith S. , et. al.: Combining Shape and Connectivity Analysis: An MRI Study of Thalamic Degeneration in Alzheimer's Disease. NeuroImage 49, Issue 1, 1-8 (2010)

[5] Fan Y., Batmanghelich N., Clark C.M y Davatzikos C.: Spatial Patterns of Brain Atrophy in MCI Patients, Identified Via High-Dimensional Pattern Classification, Predict Subsequent Cognitive Decline. NeuroImage 39, Issue 4, 1731-1743 (2008)

[6] Gerardin E., Chételat G., Chupin M., Cuingnet R., Desgranges B, et. al.: Multidimensional Classification of Hippocampal Shape Features Discriminates Alzheimer's Disease and Mild Cognitive Impairment from Normal Aging. NeuroImage 47, Issue 4, 1476-1486 (2009)

[7] Li S., Shi F., Pu F. Li X., Jiang T., et. al.: Hippocampal Shape Analysis of Alzheimer Disease Based on Machine Learning Methods. American Journal of Neuroradiology 28, 1339-1345, (2007)

[8] Lao Z., Shen D., Xue Z., Karacali B., Resnick S.M., et. al.: Morphological Classification of Brains Via High-Dimensional Shape Transformation and Machine Learning Methods. NeuroImage 21, Issue 1, 46-57 (2004)

[9] Ferrarini L., Frisoni G.B., Pievani M., Reiber J.H.C, Ganzola R., et. al.: Morphological Hippocampal Markers for Automated Detection of Alzheimer's Disease and Mild Cognitive Impairment Converters in Magnetic Resonance Images. Journal of Alzheimer's Disease 17 (3), 643-659 (2009)

[10] Chincarini A., Bosco P., Calvini P., Gemme G., Esposito M., et. al.: Local MRI Analysis Approach in the Diagnosis of Early and Prodromal Alzheimer's Disease. NeuroImage 58, Issue 2, 469-480 (2011)

[11] Davatzikos C., Bhatt P., Shaw L.M., Batmanghelich K.N. y Trojanowski J.Q.: Prediction of MCI to AD Conversion, Via MRI, CSF Biomarkers, and Pattern Classification. Neurobiology of Aging 32, Issue 12, 2322e19-2322e27 (2011)

[12] Dubois B., Feldman H.H., Jacova C., DeKosky S.T., Barberger-Gateau P., et. al.: Research Criteria for the Diagnosis of Alzheimer's Disease: Revising the NINCDS-ADRDA Criteria. The Lancet Neurology 6 (8), 734-746 (2007)

[13] Magnin B., Mesrob L., Kinkingnéhun S., Pélégrini-Isaac M., Colliot O., et. al.: Support Vector Machine-Based Classification of Alzheimer's Disease From Whole-Brain Anatomical MRI. Neuroradiology 51, 73-83 (2009)

[14] Fan Y., Batmanghelich N., Clark C.M. y Davatzikos C.: Spatial Patterns of Brain Atrophy in MCI Patients, Identified Via High-Dimensional Pattern Classification, Predict Subsequent Cognitive Decline. NeuroImage 39, Issue 4, 1731–1743 (2008)

[15] Cuingnet R., Gerardin E., Tessieras J., Auzias G. Lehéricy S., et. al.: Automatic Classification of Patients with Alzheimer's Disease from Structural MRI: A Comparison of Ten Methods Using the ADNI Database. NeuroImage 56, Issue 2, 766-781 (2011)

[16] Hinrichs C., Singh V., Mukherjee L., Xu G. Chung M.K., Johnson S.C., et. al.: Spatially Augmented LPboosting for AD Classification with Evaluations on the ADNI Dataset. NeuroImage 48, Issue 1, 138-149 (2009)

[17] Klöppel S., Stonnington C.M., Chu C., Draganski B., Scahill R.I., et. al.: Automatic Classification of MR Scans in Alzheimer's Disease. Brain 131, Issue 3, 681-689 (2008)

[18] Costafreda S.G., Dinov I.D., Tu Z., Shi Y., Lui C.Y, et. al.: Automated Hippocampal Shape Analysis Predicts the Onset of Dementia in Mild Cognitive Impairment. Neuroimage 56, Issue 1, 212-219 (2011)

[19] Vemuri P., Gunter J.L., Senjem M.L., Whitwell J.L., Kantarci K, et. al.: Alzheimer's Disease Diagnosis in Individual Subjects Using Structural MR Images: Validation Studies. NeuroImage 39, Issue 3, 1186-1197 (2008)

[20] Gutman B., Wang Y., Morra J., Toga A.W. y Thompson P.M.: Disease Classification with Hippocampal Shape Invariants. Hippocampus, Special Issue: Procedings of the Computational Hippocampal Anatomy and Physiology Workshop 19, Issue 6, 572-578 (2009)

[21] Fan Y., Shen D. y Davatzikos C.: Classification of Structural Images Via High Dimensional Image Warping, Robust Feature Extraction, and SVM. Proceedings of the 8th International Conference on Medical Image Computing and Computer-Assisted Intervention 8, 1-8 (2005)

[22] Fan Y., Shen D., Gur R.C. y Davatzikos C.: COMPARE: Classification of Morphological Patterns Using Adaptive Regional Elements. IEEE Transactions on Medical Imaging 26, Issue 1, 93-105 (2007)

[23] Fan Y., Resnick S.M., Wu X. y Davatzikos C.: Structural and Functional Biomarkers of Prodromal Alzheimer's Disease: a High-Dimensional Pattern Classification Study. NeuroImage 41, Issue 2, 277–285 (2008)

[24] Colliot O., Chételat G., Chupin M., Desgranges B., Magnin B., et. al.: Discrimination Between Alzheimer Disease, Mild Cognitive Impairment, and Normal Aging by Using Automated Segmentation of the Hippocampus. Radiology 248, Issue 1, 194–201 (2008)

[25] Morra J.H., Tu Z., Apostolova L.G., Green A.E., Avedissian C., et. al.: Validation of a Fully Automated 3D Hippocampal Segmentation Method Using Subjects With Alzheimer's Disease, Mild Cognitive Impairment, and Elderly Controls. Neuroimage 43 (1), 59–68 (2008)

[26] Yushkevich P.A., Gerig G., Soldea O., Gao, et. al.: ITK-SNAP. Obtenido en Febrero de 2014, de http://www.itksnap.org

[27] Goebel R.: Brain Innovation BV. Obtenido en Abril de 2014, de http://www.brainvoyager.com

[28] Pyle, D.: Data Preparation for Data Mining. Morgan Kaufmann Publishers, pp. 539 (1999)

[29] Mitchel T.M.: The Discipline of Machine Learning. Otained in September of 2014, from http://www-cgi.cs.cmu.edu/~tom/pubs/MachineLearningTR.pdf

[30] Tan P.N., Steinbach M. y Kumar V.: Introduction to Data Mining. Pearson Education. Primera edición (2006)

[31] Witten I.H. y Frank E.: Data Mining – Practical Machine Learning Tools and Techniques. Elsevier. Segunda edición (2005)

[32] University of Maikato: WEKA. Obtenained in July of 2014, from http://www.cs.waikato.ac.nz/ml/weka/

[33] Thompson B. y Thompson W.: Finding Rules in Data. BYTE 11, Issue 12, 149-158 (1986)